ONLINE SUPPLEMENT for *Geophys. Res. Lett.*, **34**, L05812, doi:10.1029/2006GL027305, 2007

A prototype for convective margin shifts: Supplement

B. R. Lintner and J. D. Neelin

Department of Atmospheric and Oceanic Sciences and Institute of Geophysics and Planetary Physics, University of California at Los Angeles Los Angeles, California, USA

1. Primitive equations and their vertical average

The temperature and moisture equations are:

$$(\partial_t + D_T)T + \nabla \cdot \mathbf{v}\partial_p s = Q_c + g\partial_p R^{\uparrow} - g\partial_p R^{\downarrow} - g\partial_p S + g\partial_p G_T \quad \text{(S-1)}$$

$$(\partial_t + D_q)q + \nabla \cdot \mathbf{v}\partial_p q = Q_q + g\partial_p G_q \quad \text{(S-2)}$$

where T and q are temperature and humidity (in K); $s = T + \phi$ is the dry static energy (ϕ is the geopotential); $R^{\uparrow}$ and $R^{\downarrow}$ are nonlocal upward and downward longwave radiative fluxes (in K s^{-1}); S is the net shortwave radiative flux (positive downward); Q_c and Q_q are convective heating and moistening; and G_T and G_q are turbulent fluxes of temperature and moisture (latent and sensible) heating. The operators, D_T and D_q are defined as $D_T = D_q = \mathbf{v} \cdot \nabla - K\nabla^2$, with $\mathbf{v}$ denoting horizontal wind components and K an effective horizontal eddy diffusivity.

Consider a horizontal windfield consisting of a set of vertical structures, i.e.,

$$\mathbf{v} = \sum_{k=0}^{N} V_k(p)\mathbf{v_k}(x, y, t) + \mathbf{v_R}(x, y, p, t) \quad \text{(S-3)}$$

where $V_k(p)$ is the kth vertical structure function, and $\mathbf{v_R}(x, y, p, t)$ is a residual component of the windfield not captured by the expansion (we assume here that this component is small). Substituting the expansion (S-3) into the thermodynamic equations and invoking continuity and hydrostatic balance, (S-1) and (S-2) become, upon vertical-averaging,

$$\partial_t < T > + < D_T T > + \sum_{k=0}^{N} M_{ks} \nabla \cdot \mathbf{v_k} = < Q_c > + < Q_{rad} > + H \quad \text{(S-4)}$$

$$\partial_t < q > + < D_q q > + \sum_{k=0}^{N} M_{kq} \nabla \cdot \mathbf{v_k} = < Q_q > + E \quad \text{(S-5)}$$

where $< A >$ denotes a vertical pressure average $< A >= \Delta p^{-1} \int_{pt}^{ps} A dp$ with $\Delta p = p_s - p_t$. The coefficients M_{kx} are defined as $M_{kx} = < xV_k >$. In writing these equations, the total radiative heating of the column is included in $< Q_{rad} >$, and the turbulent fluxes comprise evaporation and sensible heating (E and H) at the lower boundary. Enthalpy conservation is invoked to write $< Q_c > = - < Q_q > = P$, where P is the total convective precipitation rate.

2. Parameter values used in model simulations

The parameter values utilized in this study were taken from version 2.3 of QTCM1 [*Neelin and Zeng*, 2000; *Zeng et al.*, 2000]. To obtain the margin prototype x_c values in Figure 3 of the manuscript, $q_c(T)$ was estimated at the peak value of the land-only precipitation field at 9.4°S, 5.6°S, and 1.6°S between 70°W- 30°W. q_0, F_T, and u_q were extracted at the first land gridpoint adjacent to the ocean. For reference, the climatological values of $q_c(T)$ and q_0 for September-October-November (SON), averaged over 9.4°S-1.6°S, are 50.2 K and 47.9 K respectively. The climatological SON mean of F_T is ∼75 W m^{-2} (or 8.6x10^{-6} K s^{-1}), corresponding to $\nabla \cdot \mathbf{v} = 2.6\text{x}10^{-6}$ s^{-1} for $M_s = 3.3$ K, while the climatological low-level inflow windspeed along the coastal margin is ∼-4.6 m s^{-1}. The value of the moisture stratification parameter, M_{qp}, is 0.0507.

The length-scale $\lambda_c^{-1} = -u_q \tau_c M_s M^{-1}$ defines the scale over which the moisture and precipitation fields achieve their maximum values after the threshold $q = q_c(T)$ is exceeded. In this sense, for finite τ_c, the location of the convective margin as estimated from, say, the half maximum value reflects not only the distance over which the threshold is met (i.e., x_c) but also the transition scale to the maximum precipitation value. For the value of τ_c used in QTCM1v2.3 (i.e., 2 hours), $\lambda_c^{-1} \approx 215$ km, which is non-negligible compared to the values of x_c in Figure 3. However, since λ_c^{-1} is expected to vary little with El Niño-related climate perturbations, the perturbations of the convective margin largely reflects variations in x_c itself.

3. Anomaly spatial structures and their relationship to climatology

As noted in Section 4 of the manuscript, the climatologies of precipitation and low-level circulation over tropical South America during the September-October-November (SON) season appear well suited to application of the margin prototype as outlined (manuscript Figure 4). Figure S1 is analogous to Figure 4, except that the satellite-derived Climate Prediction Center (CPC) Merged Analysis of Precipitation (CMAP) precipitation

0094-8276/08/$5.00

product [*Xie and Arkin*, 1997] is used in place of the CAMS rain gauge data. (Note the period of data coverage is 1979-2000.) Because the CMAP data cover both land and ocean, they offer some insights not seen in the land-only CAMS data. For example, it is noted that the Atlantic coastal margin of South America from 15°S-5°N is subject to relatively dry inflow moisture values in SON since it lies to the south of the Atlantic Intertropical Convergence Zone (ITCZ). Thus, the inflow q_0 is anticipated to be relatively constant along this margin.

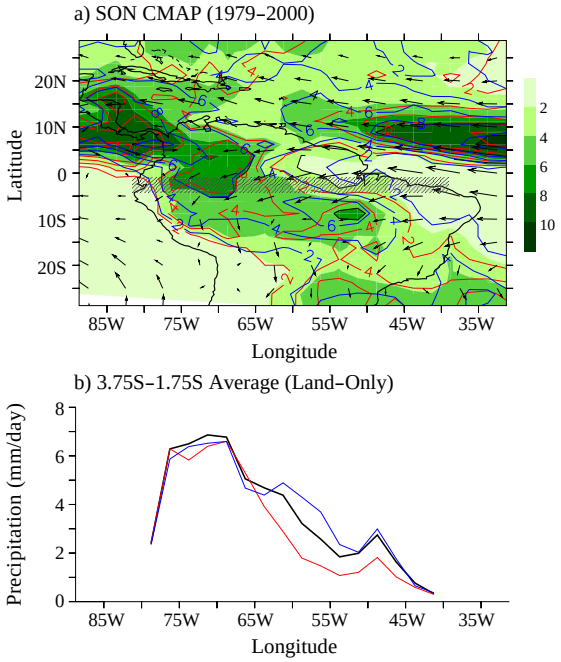

FIGURE S 1: SON composites of observed CMAP satellite precipitation for South America during 1979-2000. In (a), the El Niño phase average (red contours) consists of those years for which the SON-averaged NINO3 $\geq$ 1 standard deviation, while the La Niña phase (blue contours) consists of those years with NINO3 $\leq$ -1 standard deviation. Also shown are the mean SON CMAP precipitation over all years (filled contours; in mm day^{-1}) and the mean SON 850 mb windfield (vectors) from the NCAR/NCEP 40-year Reanalysis. Panel (b) illustrates longitudinal transects, averaged over the stippled area in (a), for El Niño (red), La Niña (blue), and all years.

To provide some perspective on situations more complex than are appropriate for the 1D prototype, Figure S2 illustrates the precipitation and wind field climatologies over South America during December-January-February (DJF). In much of the 5°S-5°N band, the DJF precipitation field increases southward toward a broad maximum near 10°S in the central interior of the continent, while a secondary maximum also occurs along the northeastern coastal margin. The 850 mb windfield includes a more northerly component, and in some regions, notably near the equator around 60°W, the prevailing flow is parallel to the mean precipitation contours. Also, because the Atlantic ITCZ lies farther south in DJF relative to SON, the inflow into the continent is likely far from uniform. In light of these features, the spatial structures of the DJF composites are arguably more complex than in SON. However, despite the complications described above, some indications of convective margin shifts are nevertheless evident in DJF, e.g., in the vicinity of 10°S, where the zonal flow is largely normal to the mean precipitation contours and the inflow originates to the south of the ITCZ.

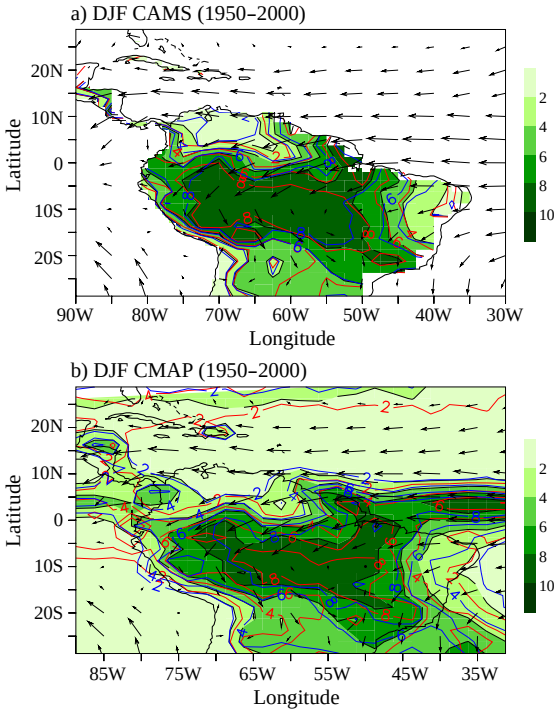

FIGURE S 2: DJF composites of observed (a) CAMS rain gauge precipitation (1950-2000) and (b) CMAP satellite precipitation (1979-2000) over tropical South America. The El Niño phase average (red contours) consists of those years for which the SON-averaged NINO3 $\geq$ 1 standard deviation, while the La Niña phase (blue contours) consists of those years with NINO3 $\leq$ -1 standard deviation. Also shown are the mean DJF precipitation fields for each dataset over all years (shaded contours; in mm day^{-1}) and the mean DJF 850 mb windfield (vectors) from the NCAR/NCEP 40-year Reanalysis.

References

Chen, M., P. P. Xie, J. E. Janowiak, and P. A. Arkin, Global land precipitation: a 50-year monthly analysis based on gauge observations. *J. Hydrometeor.* **3**, 249–266, 2002.

Kalnay, E., *et al.*, The NCEP/NCAR 40-Year Reanalysis Project, *Bul. Amer. Met. Soc.* **77**, 437–471, 1996.

Neelin, J. D., and N. Zeng, A quasi-equilibrium tropical circulation model– Formulation. *J. Atmos. Sci.* **57**, 1741–1766, 2000.

Xie, P. P., and P. A. Arkin, Global precipitation: a 17-year monthly analysis based on gauge observations, satellite observations, and numerical model output. *Bull. Amer. Meteor. Soc.* **78**, 2539–2558, 1997.

Zeng, N., J. D. Neelin, and C. Chou, A quasi-equilibrium tropical circulation model—implementation and simulation. *J. Atmos. Sci.* **57**, 1767–1796, 2000.

B. R. Lintner and J. D. Neelin Department of Atmospheric and Oceanic Sciences, and Institute of Geophysics and Planetary Physics, University of California at Los Angeles, Los Angeles, CA 90095-1565, USA (ben@atmos.ulca.edu; neelin@atmos.ucla.edu)